ACS OMEGA

Article

Cite This: ACS Omega 2019, 4, 4071−4081

http://pubs.acs.org/journal/acsodf

Recyclable Au/SiO_2-Shell/Fe_3O_4-Core Catalyst for the Reduction of Nitro Aromatic Compounds in Aqueous Solution

Kushanava Bhaduri,[†,⊥] Bidya Dhar Das,[†,⊥] Rawesh Kumar,[‡,#] Sujan Mondal,[§] Sauvik Chatterjee,[§] Sneha Shah,[†] Juan J. Bravo-Suárez,*[,∥] and Biswajit Chowdhury*[,†]

[†]Department of Applied Chemistry, Indian Institute of Technology (ISM), Dhanbad, Dhanbad 826004, Jharkhand, India

[‡]Department of Chemistry, Sankalchand Patel University, Visnagar 384315, Gujarat, India

[§]Department of Materials Science, Indian Association for the Cultivation of Science, Kolkata 700032, India

[∥]Chemical and Petroleum Engineering Department, Center for Environmentally Beneficial Catalysis, The University of Kansas, Lawrence, Kansas 66045, United States

Supporting Information

ABSTRACT: Highly stable gold nanoparticles immobilized on the surface of amine-functionalized nanocomposite microspheres possessing a magnetite (Fe_3O_4) nanoparticle core and a silica (SiO_2) shell (Au/SiO_2-shell/Fe_3O_4-core) were prepared. These gold nanocomposite catalysts were tested for 4-nitrophenol (4-NP) and 2-nitroaniline (2-NA) reduction in aqueous solution in the temperature range 293−323 K and in the presence of aqueous $NaBH_4$ reducing agent. The magnetically recyclable gold catalyst showed high stability (~3 months), efficient recyclability (up to 10 cycles), and high activity (~100% conversion within 225 s, ~700 ppm 4-NP or 2-NA). The pseudo-first-order apparent reaction rate constants (k) of 4-NP and 2-NA reduction were 7.5×10^{-3} and 4.1×10^{-3} s^{-1}, respectively, and with an apparent catalytic activity of 4.48×10^{-8} kmol/(m^3 s).

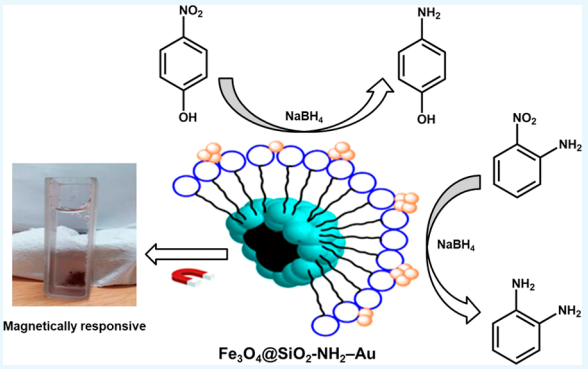

1. INTRODUCTION

Removal of organic dye pollutants such as nitro-derived aromatic compounds from wastewater is a major challenge for chemical industries and many localities worldwide. The United States Environmental Protection Agency has declared 4-nitrophenol (4-NP) and 2-nitroaniline (2-NA) as high-priority toxic pollutants because they are readily soluble in water and harmful to aquatic life.[1,2] Nitro aromatic compounds such as 4-NP and 2-NA are extensively used as chemicals for industries in everyday life. They play a major role in the manufacturing of pharmaceuticals, pigments, dyes, plastics, pesticides and fungicidal agents, explosives, and industrial solvents. For example, 4-NP is one of the nitro aromatic compounds which is an intermediate in the synthesis of paracetamol and as raw material for fungicides.[3] Similarly, 2-NA reduction also received great attention owing to its applications in dye, rubber, and textile industries.[4] 2-NA is also a starting material for elastomers, aramid textile fibers, and thermoplastics.[5] However, these notorious chemicals are highly hazardous for the environment and also toxic toward humans, animals, and plants.[6] Therefore, from both industrial and environmental points of view, reduction of 4-NP and 2-NA is of utmost importance. For the transformation of such harmful chemicals, a significant amount of research has been done so far, with most of the established methods being based on wet air oxidation,[7] electrochemical reduction,[8,9] biodegradation method,[10,11] and catalytic reduction.[6,12−15] Among the various existing investigations, catalytic reduction methods were found to be the most promising ones[16,17] as the use of a catalyst enhanced the electron transfer between the reductant and the acceptor nitro aromatic compound. Over the past decades, metal nanoparticles (NPs) have been used extensively as catalysts for several reactions and received much attention due to their high catalytic activity. The high surface area-to-volume ratio, high surface energy, and Fermi potential of metal nanoparticles make them suitable for use in catalysis.[6,18−20] It is well established that at the nanoscale size noble metals are particularly effective for catalytic conversion.[21] A prototypical example is that of gold, which is inactive when present in bulk but becomes active in the form of nanoparticles (NPs), as demonstrated for a number of gold NP-catalyzed reactions including CO oxidation,[21] propylene epoxidation,[22,23] acetylene hydrochlorination,[24] glycerol oxidation,[25] and alcohol oxidation.[26] Although it has been reported that metal nanoparticles in homogeneous reaction media show higher catalytic activities than those of their corresponding heteroge-

Received: December 28, 2018
Accepted: February 11, 2019
Published: February 22, 2019

DOI: 10.1021/acsomega.8b03655
ACS Omega 2019, 4, 4071−4081

neous supported counterparts,[27] their separation from the reaction medium and the possibility of product contamination are major challenges. For heterogeneous systems, gold nanoparticles have been usually dispersed on supports such as carbon,[28] metal oxides,[29] and zeolites.[30] Metal oxide-supported gold nanoparticles, for example, have been widely used for CO oxidation (even at subambient temperatures) as well as for propylene epoxidation using hydrogen and oxygen mixtures.[23] For these reactions, the catalytic activity has been shown to be highly dependent on gold particle size, with smaller nanoparticles commonly being more active. Another major challenge with supported catalysts possessing small particle sizes and in liquid phase reactions is that metal NPs tend to sinter and leach if metal and support interactions are weak. Therefore, methodologies for immobilization of metal nanoparticles on solid supports to minimize this complication have been usually explored.[31]

The additional presence of Fe nanoparticles in novel metal-supported catalytic systems has also been found to be advantageous as it provides magnetic separability from the reaction medium.[32,33] However, as-synthesized Fe_3O_4 metal NPs are not stable due to their high surface energy, which strongly favors their aggregation, decomposition, and oxidation.[32] One approach to avoid these issues is to protect Fe_3O_4 NPs with a shell of tunable thickness of a different material. Such an approach has been explored by Duan et al.[34] who synthesized Fe-glycerate hollow nanospheres, followed by a coating of polydopamine (Fe@PDA) and immobilization of novel metal Pd over the double-shell hollow nanospheres. Chang et al.[1] also fabricated Au nanoparticles over chitosan-coated Fe_3O_4 nanocarriers, whereas Mohammadi et al.[35] decorated Ag NPs over silica-coated iron oxide using safflower extract for nitrophenol reduction. In another approach, Zheng et al.[36] immobilized AuNPs on synthesized Fe_3O_4@SiO_2 (SiO_2-shell/Fe_3O_4-core) via added surface Sn^{2+} linking followed by reduction. Metal NPs supported on Fe_3O_4 and Fe_3O_4@SiO_2 materials have also been prepared via support functionalization by $-NH_2$ groups and applied toward 4-NP reduction[23,37−39] along with 2-NA reduction.[40,41] Deposition of metal NPs has also been explored on SiO_2 surfaces as reduction catalysts.[42,43] Therefore, SiO_2-shell/Fe_3O_4-core materials are expected to be excellent supports for stabilization of metal NPs.[35] However, in most of the cases, catalyst performance was incomplete as a comparison was based on the reaction completion time rather than on more rigorous normalized reaction rates (e.g., per unit surface area of the catalyst) or reaction rate constants.

Although 4-NP reduction has been widely studied, its counterpart, 2-NA, reduction has not received as much attention despite its environmental and industrial relevance. Herein, we introduce a system composed of Au nanoparticles supported on amino-functionalized SiO_2-shell/Fe_3O_4-core microspheres (Au/(NH_2)SiO_2-shell/Fe_3O_4-core) with catalytic properties for the reduction of nitro aromatic compounds, which can be magnetically recoverable from the reaction medium. The Au/(NH_2)SiO_2-shell/Fe_3O_4-core materials were characterized by nitrogen physisorption (i.e., for surface area and porosity), X-ray diffraction (XRD), high-resolution transmission electron microscopy (HR-TEM), and Fourier transform infrared spectroscopy (FTIR) techniques, and their catalytic activity was evaluated for the reduction of 4-NP and 2-NA in the aqueous phase at near-ambient conditions. The obtained results show the role of gold nanoparticles in the catalytic reduction and support surface functionalization as a viable strategy for nanoparticle deposition and the use of SiO_2-shell/Fe_3O_4-core materials as adequate materials for catalyst recovery during the conversion of nitro-derived compounds present in aqueous solutions.

2. RESULTS AND DISCUSSION

2.1. Catalyst Characterization. From Figure 1, the XRD patterns of Fe_3O_4, SiO_2-shell/Fe_3O_4-core (Fe_3O_4@SiO_2), (NH_2)SiO_2-shell/Fe_3O_4-core (Fe_3O_4@SiO_2-NH_2), and Au/(NH_2)SiO_2-shell/Fe_3O_4-core (Fe_3O_4@SiO_2-NH_2−Au) materials can be seen. The XRD patterns of Fe_3O_4 nanoparticles display intense 2θ peaks at about 30.1, 35.4, and 43.1°, which are assigned to the (220), (311), and (400) planes, respectively. These peaks indicate that Fe_3O_4 nanoparticles present a crystalline cubic spinel structure of magnetite (JCPDS no. 00-019-0629). The XRD pattern of the SiO_2-shell/Fe_3O_4-core sample shows a broad diffraction peak at 2θ = 20−30° due to the existence of amorphous silica.[44] In this sample, the peak intensities corresponding to the (220), (311), and (400) planes of cubic Fe_3O_4 are almost indistinguishable after silica coating as a result of dilution and reduced X-rays interaction with Fe_3O_4. Furthermore, the XRD patterns of Au/(NH_2)SiO_2-shell/Fe_3O_4-core are indexed by weak peaks due to cubic Fe_3O_4 and gold cubic phase (two peaks at 2θ values of 38.2 and 44.4° due to the (111) and (200) planes, JCPDS card no. 00-004-0784).

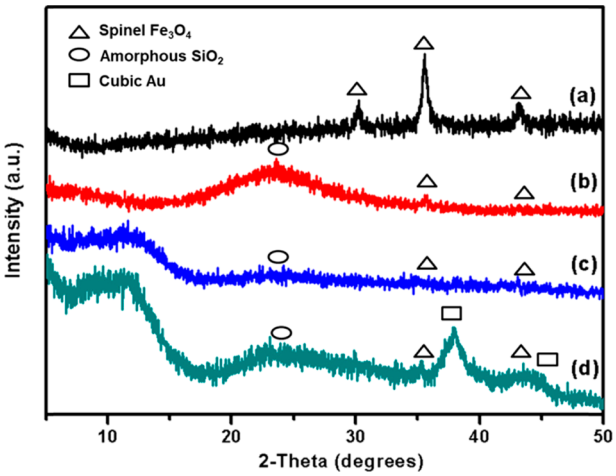

Figure 1. Wide-angle powder X-ray diffractograms of (a) Fe_3O_4 particles, (b) Fe_3O_4@SiO_2 microspheres, (c) Fe_3O_4@SiO_2-NH_2, and (d) Fe_3O_4@SiO_2-NH_2−Au catalyst.

The N_2 adsorption−desorption isotherms of Fe_3O_4@SiO_2-NH_2−Au and the corresponding support materials are shown in Figure 2, whereas their surface areas and average pore diameters are summarized in Table 1. The Fe_3O_4 isotherm can be classified as a type IV with an H2 hysteresis loop in the relative pressure range of 0.1−0.5, which indicates the presence of mesopores formed during the agglomeration of Fe_3O_4 NPs. Such agglomeration is also reflected in the small observed Brunauer−Emmett−Teller (BET) specific surface area of 24 m^2/g and an average pore size of 3.0 nm. As expected, the SiO_2-shell/Fe_3O_4-core magnetic microspheres (Fe_3O_4@SiO_2) also possess similar textural properties (type-IV isotherm, H2 hysteresis) characteristic of mesoporous materials.[45] The higher surface area (53 m^2/g) of the Fe_3O_4@SiO_2 sample

DOI: 10.1021/acsomega.8b03655
ACS Omega 2019, 4, 4071−4081

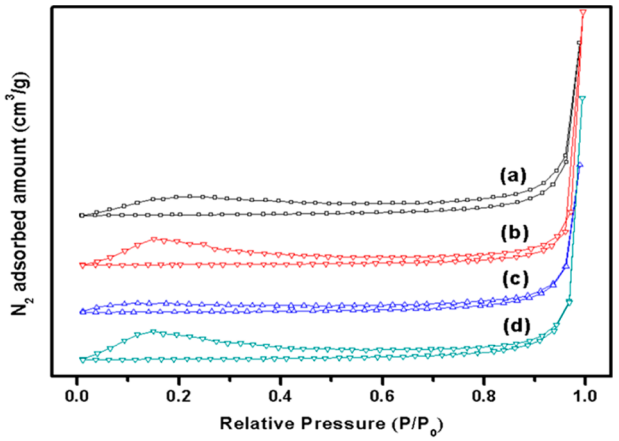

Figure 2. N_2 adsorption−desorption isotherms of (a) Fe_3O_4 particles, (b) Fe_3O_4@SiO_2 microspheres, (c) Fe_3O_4@SiO_2-NH_2, and (d) Fe_3O_4@SiO_2-NH_2−Au catalyst.

Table 1. BET Surface Area and Pore Size Results of Prepared Materials

material	BET surface area (m^2/g)	average pore diameter (nm)
Fe_3O_4	24	3.0
Fe_3O_4@SiO_2	53	3.1
Fe_3O_4@SiO_2-NH_2	111	3.4
Fe_3O_4@SiO_2-NH_2−Au	62	3.3

with respect to that of Fe_3O_4 is the result of the presence of SiO_2 whose specific surface area and pore size should be larger than those of Fe_3O_4. Also, the SiO_2 shell should help reduce the agglomeration of Fe_3O_4, freeing void space among particles. After the $-NH_2$ functionalization, the surface area increased to 111 m^2/g. It is not clear at present why there is a significant increase in surface area with respect to that of the parent Fe_3O_4@SiO_2, but we speculate that the high-temperature hydrothermal treatment may have opened additional pores in the SiO_2 shell, making them available for N_2 adsorption, as suggested by the larger observed average pore size (3.4 nm). Such pores, however, are blocked upon significant Au deposition on the SiO_2 surface, thus reducing the surface area from 111 to 62 m^2/g in the final Au/$(NH_2)SiO_2$-shell/Fe_3O_4-core catalyst. The Au loading on the Au/$(NH_2)SiO_2$-shell/Fe_3O_4-core catalyst obtained from energy dispersive X-ray spectroscopy (EDS) measurements was 3.4 wt %, confirming that gold was incorporated in the Fe_3O_4@SiO_2-NH_2−Au catalyst.

Figures 3 and 4 display the HR-TEM images of SiO_2-shell/Fe_3O_4-core and Au/(NH_2)/SiO_2-shell/Fe_3O_4-core catalyst NPs with a mean diameter of 440 ± 40 nm. It has been reported that the shape and size of Fe_3O_4 NPs are difficult to control during synthesis.[46] Figure 3a shows an example of the multiagglomerates of SiO_2-shell/Fe_3O_4-core that can still form. This is an inherent challenge for the synthesis of magnetic core−shell nanocomposites of uniform size distribution; nevertheless, the ultimate goal of preparing SiO_2-shell/Fe_3O_4-core nanocomposites that are easily recoverable is shown to be feasible (Figure 3) and is demonstrated in Figure 3d, which shows the presence of both Si and Fe on the SiO_2/Fe_3O_4 support.

It has been revealed that the obtained Fe_3O_4−SiO_2-NH_2−Au catalyst has an average AuNP diameter of 6.7 ± 1.6 nm, which is distributed homogeneously over the support surface. The existence of Fe, Si, and Au is also demonstrated in the EDS spectra of the support and catalyst NPs in Figures 3d and 4f. These results indicate a strong interaction of the gold NPs with the NH_2-SiO_2-shell/Fe_3O_4-core support enabled by the amine surface modification. The surface of the functionalized SiO_2 coating in the core−shell Fe_3O_4@SiO_2 microspheres consists mainly of NH^{3+} and unmodified Si−OH groups. Upon gold deposition on the SiO_2 surface, the negatively charged $AuCl^{4-}$ gold precursor interacts preferentially with the $-NH_3^+$ groups through electrostatic attraction and thus resulting in an

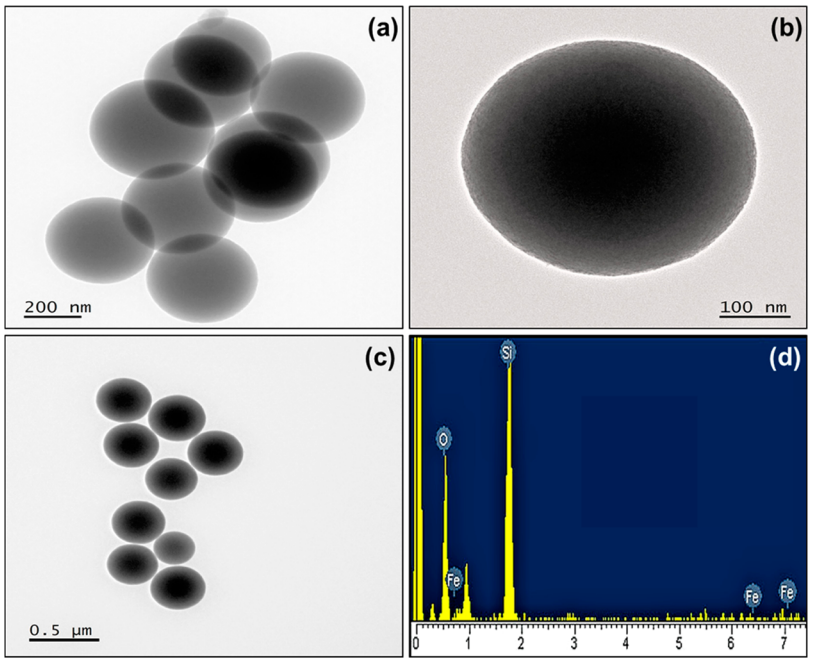

Figure 3. High-resolution TEM images (a−c) and EDS spectra (d) of Fe_3O_4@SiO_2 microspheres.

DOI: 10.1021/acsomega.8b03655
ACS Omega 2019, 4, 4071−4081

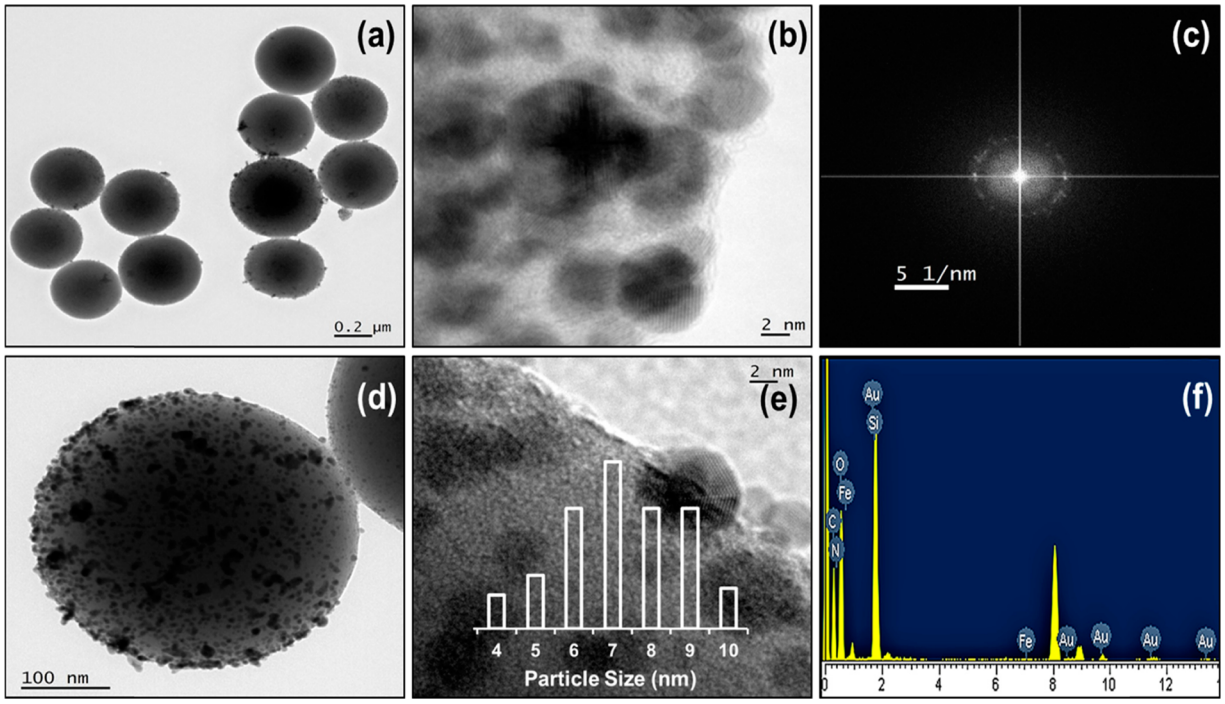

Figure 4. High-resolution TEM images (a–e), selected area electron diffraction pattern (c), and EDS spectra (f) of Fe_3O_4@SiO_2-NH_2–Au core–shell microspheres. The inset in (d) shows the Au particle size distribution.

almost quantitative deposition of gold over the whole silica surface, which is highly crystalline in nature (Figure 4c).[40]

The transmission FTIR spectra of Fe_3O_4, Fe_3O_4@SiO_2, Fe_3O_4@SiO_2-NH_2, and Fe_3O_4@SiO_2-NH_2–Au in the 4000–400 cm^{-1} range are shown in Figure 5. The band in the region

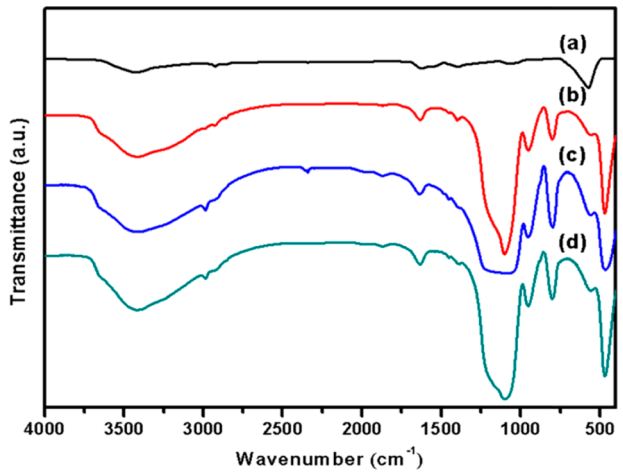

Figure 5. FTIR spectra of (a) Fe_3O_4 particles, (b) Fe_3O_4@SiO_2 microspheres, (c) Fe_3O_4@SiO_2-NH_2, and (d) Fe_3O_4@SiO_2-NH_2–Au catalyst.

of 585 cm^{-1} is assigned to the stretching vibration of Fe–O bonds.[47] The bands in the regions of 3400 and 1632 cm^{-1} indicate O–H and H–O–H bond vibrations of surface-adsorbed water molecules. In the case of Fe_3O_4@SiO_2, Fe_3O_4@SiO_2-NH_2, and gold-deposited Fe_3O_4@SiO_2-NH_2 materials, the peak intensity in the hydroxyl region (3400–3600 cm^{-1}) increased sharply as a result of a combination of the stretching vibration of silanol groups or hydrogen bonding as well as the axial deformation of Si–OH groups present on the SiO_2 surface.[48] The band at 1107 cm^{-1} is attributed to the asymmetric stretching vibration of framework Si–O–Si bridges, whereas the peak at 950 cm^{-1} has been assigned to the stretching vibration of Si–OH and Si–$O^{\delta-}$ groups. The peak at 803 cm^{-1} can be ascribed to the Si–O–Si symmetric stretching and successive formation of the Si–O–Fe moiety.[44] The slight decrease of peak intensity at 803 cm^{-1} with gold loading suggests a strong interaction of AuNPs with silica. Additionally, a new band at 2930 cm^{-1} in the Fe_3O_4@SiO_2-NH_2 and Fe_3O_4@SiO_2-NH_2–Au samples indicates the presence of $-NH_2$ vibration.[49] Therefore, these results overall indicate that 3-aminopropyltriethoxysilane (APTES), which is a SiO_2 surface modifier, was successfully attached to the Fe_3O_4@SiO_2 surface and remained after Au deposition.

2.2. Catalytic Activity and Stability. To check the catalyst activity performance, the reduction reactions of 4-nitrophenol (4-NP) and 2-nitroaniline (2-NA) in the presence of $NaBH_4$ were chosen as test reactions. Table 2 summarizes

Table 2. Catalytic Performance of the Fe_3O_4@SiO_2-NH_2–Au Catalyst in the Aqueous Phase Reduction of 4-Nitrophenol and 2-Nitroaniline[a]

entry	catalyst	substrate	100% conv. time (min)
1	Au/Fe_3O_4	4-NP	4.30
2	Au/SiO_2	4-NP	4.15
3	Au/NH_2-SiO_2-shell/Fe_3O_4-core	4-NP	3.75
4	Au/Fe_3O_4	2-NA	4.80
5	Au/SiO_2	2-NA	4.65
6	Au/NH_2-SiO_2-shell/Fe_3O_4-core	2-NA	4.20

[a]Reaction conditions: 0.1 cm^3 of aqueous 4-NP or 2-NA solution (5×10^{-3} M, 696 ppm), 1.0 cm^3 of freshly prepared $NaBH_4$ (0.2 M) solution, 2 cm^3 ultrapure water, 3 mg of catalyst, 303 K reaction temperature.

DOI: 10.1021/acsomega.8b03655
ACS Omega 2019, 4, 4071–4081

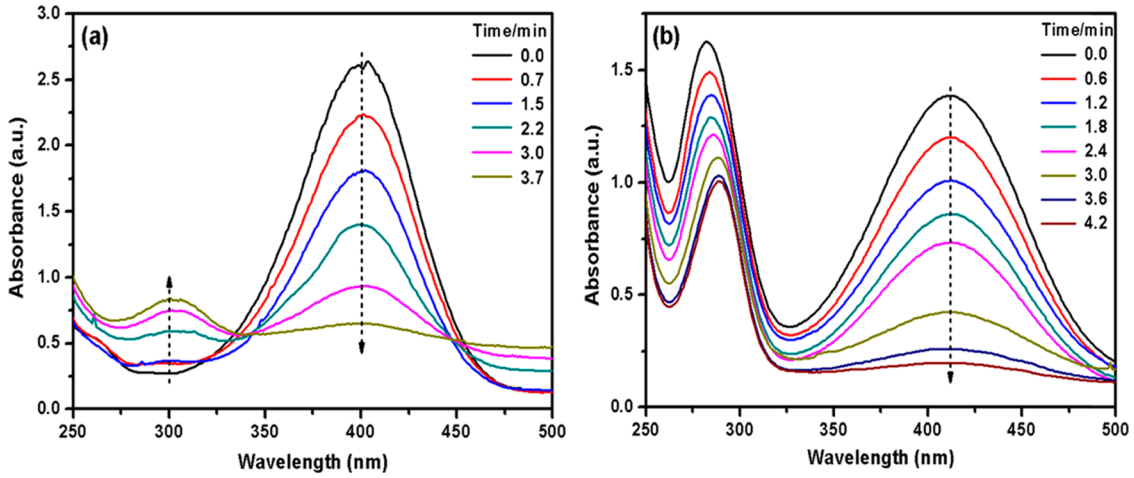

Figure 6. Time progression of UV−vis spectra during reduction of (a) 4-NP and (b) 2-NA. Reaction conditions: 0.1 cm^3 of aqueous 4-NP or 2-NA solution (5×10^{-3} M, 696 ppm), 1.0 cm^3 of freshly prepared $NaBH_4$ (0.2 M) solution, 2 cm^3 ultrapure water, 3 mg of catalyst weight, 303 K reaction temperature.

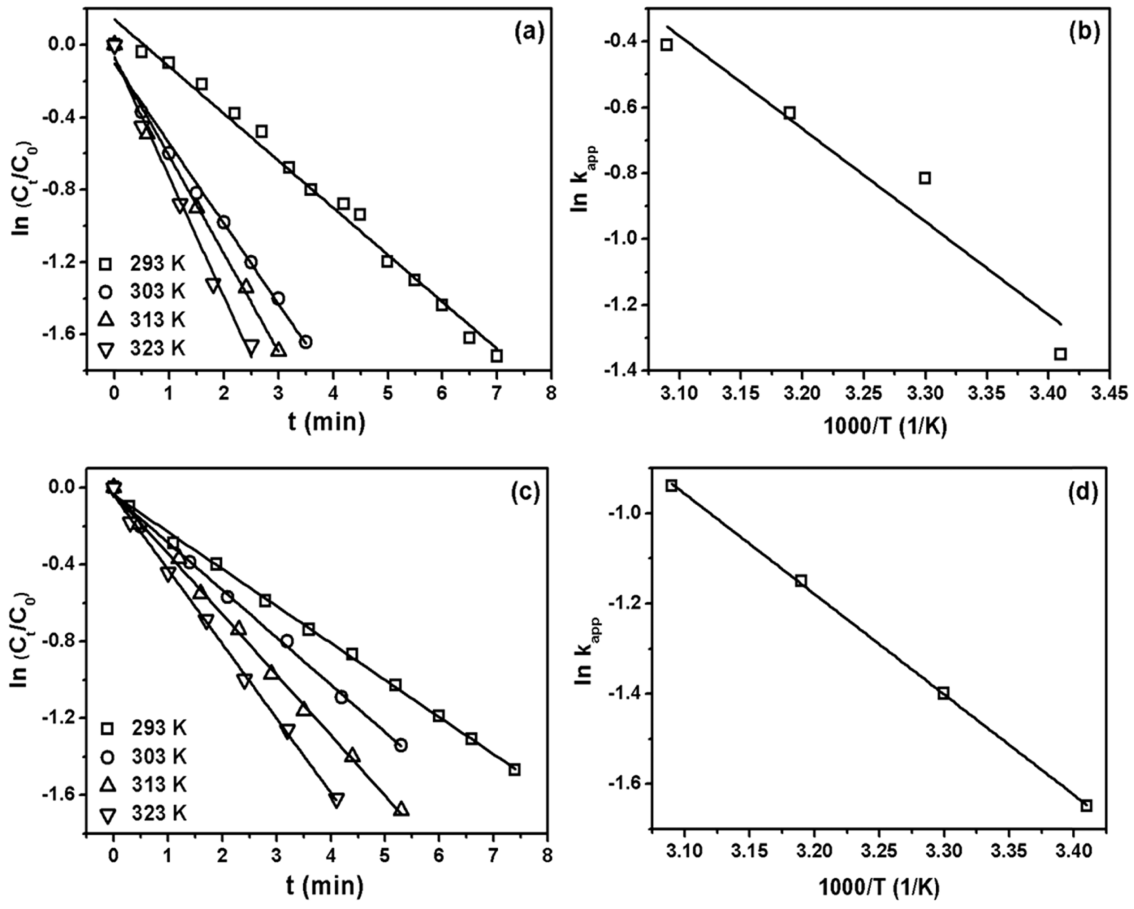

Figure 7. Fe_3O_4@SiO_2-NH_2−Au catalyst reactivity results: (a, c) relationships between $\ln(C_t/C_0)$ and reaction time (t) at four different temperatures for 4-NP and 2-NA, respectively; (b, d) plots of $\ln k_{app}$ versus $1/T$ for 4-NP and 2-NA, respectively. The black lines correspond to the best straight line fit.

the 4-NP and 2-NA complete conversion results for the Au/NH_2-SiO_2-shell/Fe_3O_4-core catalyst. It can be seen that all gold catalysts are active for the reduction of nitro aromatic compounds, with the SiO_2 support performing slightly better than Fe_3O_4. The tendency of Fe_3O_4 to agglomerate and the slightly higher activity of SiO_2-supported gold NPs, therefore, justify the use of a magnetically recoverable catalyst based on a SiO_2-shell/Fe_3O_4-core composite. The corresponding Au/SiO_2-shell/Fe_3O_4-core catalyst, as expected, resulted in a catalyst more active than Au/Fe_3O_4.

The catalytic activity of Au/NH_2-SiO_2-shell/Fe_3O_4-core was further investigated in the reduction of 4-NP and 2-NA as a function of residence time as monitored by UV−vis spectroscopy (Figure 6). UV−vis spectroscopy was used because of its

DOI: 10.1021/acsomega.8b03655
ACS Omega 2019, 4, 4071−4081

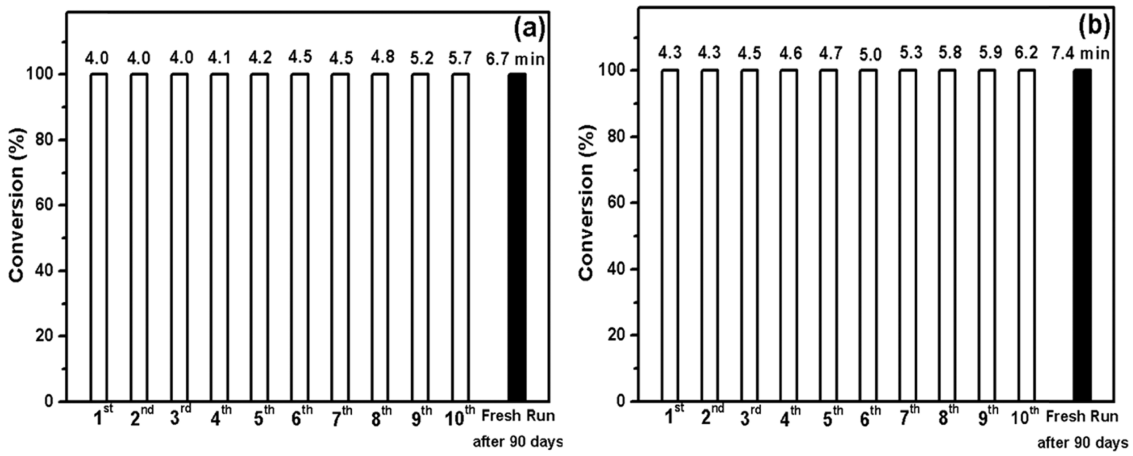

Figure 8. Recycling tests of the Fe_3O_4@SiO_2-NH_2−Au catalyst for 10 successive runs and a fresh run after a long storage time (around 90 days after the catalyst synthesis) for (a) 4-NP and (b) 2-NA. Reaction conditions: 0.1 cm^3 of aqueous 4-NP or 2-NA solution (5×10^{-3} M, 696 ppm), 1.0 cm^3 of freshly prepared $NaBH_4$ (0.2 M) solution, 2 cm^3 of ultrapure water, 3 mg of catalyst, 303 K reaction temperature.

Table 3. Comparison of Catalytic Performance of the Fe_3O_4@SiO_2-NH_2−Au Catalyst with State-of-the-Art Catalysts for the Liquid Phase Reduction of 4-Nitrophenol to 4-Aminophenol[a]

no.	catalyst	Au synthesis method	reaction conditions	completion of reaction (min)	k_{app} (s^{-1})	refs
1	Au(0)@TpPa-1 (5 ± 3 nm)	COF framework, $NaBH_4$	S = 0.18 mM (15 mL) R = 0.07 M (12 mL) C = 20 mg	13	5.3×10^{-3}	3
2	Au−CeO_2@ZrO_2 (15 nm)	PVP, $NaBH_4$	S = 1 mM (0.3 mL) R = 1 mM (3.7 mL) C = 1.4 mg/mL (0.1 mL)	21	2.4×10^{-2}	50
3	Fe@Au−ATPGO (10−12 nm)	ascorbic acid reduction method, pH = 4	S = 1.0×10^{-4} M (25 μL) R = 0.06 M (2.5 mL) C = 1.4 g/L	18	8.2×10^{-6}*	51
4	Au−DEND550-1 (3.2 nm)	organic ligand, $NaBH_4$	S = 0.09 μmol in 2.5 mL R = 7.2 μmol C = 0.5%, 0.45×10^{-3} μmol	4.6	5.1×10^{-3}	52
5	Mn@SiO_2_NH_2@Au (5 nm)	APTES, citric acid	S = 0.05 mM (3 mL) R = 0.15 mmol C = 3 mg	12	6.1×10^{-3}	53
6	AuDSNs (2.6 nm)	glycodendrimer, $NaBH_4$	S = 6.2×10^{-4} M R/S = 81:1 (equiv)	7.7	6.5×10^{-3}	54
7	KCC−1-IL/Au (2−5 nm)	KCC−1-IL, $NaBH_4$	S = 1 mM (187 μL) R = 0.1 M (2.5 mL) C = 0.5 mg/mL (25 μL)	4.5	12×10^{-3}	60
8	Fe_3O_4@SiO_2-NH_2−Au (6.7 nm)	APTES, $NaBH_4$	S = 0.1 mL (0.005 M) R = 1 mL (0.2 M), C = 3 mg	3.7	7.8×10^{-3}	this study

[a] S: substrate (i.e., 4-NP); R: reductant ($NaBH_4$); C: catalyst; k_{app} = apparent rate constant; * mol/(L min).

convenience, as bands for reactant and products can be easily discerned in the spectra. In the case of 4-NP reduction (Figure 6a), two absorption bands are observed, one at 398 nm and another at 298 nm, which are assigned to 4-NP and 4-aminophenol (4-AP reduction product), respectively. At the studied reaction conditions, it can be seen that after the addition of catalyst (~3 mg of Au/NH_2-SiO_2-shell/Fe_3O_4-core, $t > 0$), the band due to 4-NP (398 nm) progressively disappeared, whereas the band due to 4-AP (298 nm) gradually evolved until reaching a maximum after around 3.75 min, indicating near-complete reduction of 4-NP to 4-AP. In the reduction of 2-NA, two bands at 411 and 282 nm corresponded to 2-NA, whereas a band at 290 nm was due to *o*-phenylenediamine (*o*-PA) (Figure 6b). Similar to 4-NP reduction, 2-NA was reduced as indicated by a decrease in the main 411 nm band, which extinguished after around 4.20 min, indicating full conversion into *o*-PA, as shown by the remaining large band at 290 nm. It is worth noticing that these reactions did not proceed in the presence of the bare supports SiO_2-shell, Fe_3O_4-core, or SiO_2-shell/Fe_3O_4-core, indicating that gold NPs are essential for the reduction of nitro aromatic compounds. The apparent conversion rates at 4-NP and 2-NA complete reduction were calculated to be $(\sim 1.1-1.2) \times 10^{-2}$ (mol substrate/mol surface Au/s).

Additional 4-NP and 2-NA reduction tests with the Au/NH_2-SiO_2-shell/Fe_3O_4-core catalyst were performed at several near-ambient temperatures as shown in Figure 7. For comparison purposes, temporal reactivity tests, such as those

DOI: 10.1021/acsomega.8b03655
ACS Omega 2019, 4, 4071−4081

Table 4. Comparison of Catalytic Performance of the Fe_3O_4@SiO_2-NH_2−Au Catalyst with the Liquid Phase Reduction of 2-Nitroaniline to *o*-Phenylenediamine

no.	catalyst	Au synthesis method	reaction conditions	completion of reaction (min)	k_{app} (s^{-1})	refs
1	Ni@Au/KCC-1	MPTES, $NaBH_4$	S^* = 0.126 mM/L (40 μL) R = 0.5 M, 0.65 10^{-4} mol (0.13 mL) C = 10.0 mg/mL (30 μL)	10	4.7×10^{-3}	31
2	AuNPs having different shapes (60−270 nm)	PVP, $NaBH_4$	S = 0.30 mM (50 mL) R = 38 mM (50 mL) C = 0.97 mg	6−18	NM	55
3	gold nanocubes (61 nm), octahedra (45 nm), and rhombic dodecahedra (44 nm)	CTAC, $NaBH_4$	S = 1.0 mM (500 μL) R = 0.1 M (1.2 mL) C = 102 μL for nanocubes, 95 μL for octahedra, and 347 μL for rhombic dodecahedra	70 240 50	3.1×10^{-4} 6.7×10^{-5} 1.3×10^{-3}	61
4	Sr/Alg/CMC/GO/Au	$NaBH_4$	S^* = 0.1 mM (1 mL) R = 0.1 M (1 mL) C = 1 mg/mL	2	4.9×10^{-3}	62
5	Au-NF (50−70 nm)	ascorbic acid, CH-CF, KBH_4	S = 1 mM/L (300 μL) R = 0.1 M/L (300 μL) C = 0.4 mmol/L (300 μL)	16	NM	63
6	Fe_3O_4@SiO_2-NH_2−Au (6.7 nm)	APTES, $NaBH_4$	S^* = 0.1 mL (0.005 M) R = 1 mL (0.2 M) C = 3 mg	4.2	4.1×10^{-3}	this study

[a] S: substrate (i.e., 4-NA); S^*: (2-NA); R: reductant ($NaBH_4$); C: catalyst; k_{app} = apparent rate constant; * mol/(L min); NM: not mentioned.

shown in Figure 7, were analyzed assuming a pseudo-first-order kinetics via $\ln(C_t/C_o)$ vs residence time plots to evaluate the apparent reaction rates. The pseudo first order fitted reasonably well to nearly 99% of the conversion of the reactions. The corresponding apparent reaction rate constants, denoted here k_{app}, as a function of temperature are shown in Figure 7b,d. A linear relationship was found between $\ln(k_{app})$ and $1/T$. The apparent rate constant (k_{app}) values obtained under the same reaction conditions at 293, 303, 313, and 323 K were 4.3×10^{-3}, 7.4×10^{-3}, 9.0×10^{-3}, and 11.0×10^{-3} s^{-1}, respectively, for 4-NP reduction and 3.2×10^{-3}, 4.1×10^{-3}, 5.2×10^{-3}, and 6.5×10^{-3} s^{-1}, respectively, for 2-NA reduction. The obtained apparent activation energies were 24.6 and 18.4 kJ/mol for 4-NP and 2-NA reduction, respectively.

To further evaluate the stability and recyclability of the catalyst for 4-NP and 2-NA reduction, continuous runs were carried out after (magnetically) recovering the Au/NH_2-SiO_2-shell/Fe_3O_4-core catalyst (by simply placing a magnet to the side of the reaction container while the reacted solution was taken off), followed by washing with water, which was reused in the next cycle. The experimental results for 10 successive recycling reactions, as shown in Figure 8, demonstrated that the catalyst did not undergo any appreciable change in its activity and only a small drop in reaction time for complete conversion was noticed during the 10 cycles (4.0−5.7 min for 4-NP and 4.3−6.2 min for 2-NA). More remarkably, even after 90 days of storage, the catalyst efficiently carried out 100% conversion of 4-NP and 2-NA within 6.8 and 7.5 min, respectively.

The catalytic performance of the Au/NH_2-SiO_2-shell/Fe_3O_4-core catalyst was compared to that of previously reported catalysts for the same reaction, as shown in Tables 3 and 4, respectively. The results in these tables indicate that the synthesized Au/NH_2-SiO_2-shell/Fe_3O_4-core catalyst exhibited comparable or better catalytic activity (and time for 100% reaction completion) for 4-NP and 2-NA reduction than that of other reported catalysts. However, it is generally accepted that catalytic performance depends on metal NP size, active site density, stability, and metal−support interaction.[50−55] The data presented in Tables 3 and 4 suggest that the reduction of nitro aromatic compounds in the aqueous phase by gold-based catalysts appears to be dominated by the size of gold NPs and nature of the gold−support interface.

In gold catalysis, the effect that particle size has on catalytic activity is well known; however, the reasons for this are still a matter of debate. Many different hypotheses have been put forward including electronic exposure of gold sites of given coordination, etc., which appear to be dependent on the reaction under study.[56] For example, in gas phase reactions with supported gold catalysts, it appears that there is a gold nanoparticle size (and not necessarily the same) at which an optimum number of active sites exist at the support−metal particle interface that effectively catalyze several reactions such as the water−gas shift and CO oxidation reaction.[56,57] In liquid phase reactions, the situation is more complex as solvent molecules can solvate around gold nanoparticles to different extents and block or facilitate access to gold active sites. This effect is evident, for example, in prior reports for reduction of 4-NP by AuNPs (5, 9, 11, and 19 nm) supported by polyphenol grafting on collagen fibers.[58] Although all catalysts exhibited catalytic activity for 4-NP reduction even with particles as large as 19 nm, an optimum activity was found with the 11 nm AuNP catalyst. This high value of activity was hypothesized to be due to optimum access to gold active sites because of lower steric hindrance of the polyphenol grafting agent that remained on the catalyst surface.[58] Similar particle size effects were also observed for 4-NP reduction with colloidal AuNPs and Al_2O_3 supported Au (2.0, 3.4, 5.7, and 8.2 nm) catalysts, which resulted in optimum particle sizes of 3.4 nm for the former and between 3.4 and 5.7 nm for the latter.[59] The average gold particle size in the Fe_3O_4@SiO_2-NH_2−Au catalyst is relatively large (6.7 nm) with respect to that in some

DOI: 10.1021/acsomega.8b03655
ACS Omega 2019, 4, 4071−4081

colloidal AuNPs in Table 3 (e.g., nos. 4 and 6) but within the previously reported optimum Au range for Au/Al_2O_3.[59] This apparent discrepancy of higher activity in the Fe_3O_4@SiO_2-NH_2−Au catalyst with respect to that in the colloidal AuNPs could also be explained by steric hindrance because of the presence of larger organic ligands that impede diffusion of reactants to the Au surface, something that is not present in the Fe_3O_4@SiO_2-NH_2−Au catalyst prepared in this work.

3. CONCLUSIONS

In conclusion, we demonstrated the successful preparation of multifunctional magnetic Au/NH_2-SiO_2-shell/Fe_3O_4-core nanocomposite microspheres of a magnetite particle (Fe_3O_4) core with a well-defined silica-protected shell and the deposition of active AuNPs of approximately 6.7 ± 1.6 nm on the outer shell of $-NH_2$-functionalized SiO_2-shell/Fe_3O_4-core. The synthetic procedure for the functionalization of the nanocomposite catalyst was relatively simple, allowing it to also be easily separable by an external magnet from the reaction environment. The experimental reaction rates, apparent reaction rate constants, and activation energies showed that the catalytic reduction of 4-nitrophenol and 2-nitroaniline at the studied conditions was complete within several minutes with similar or better performance than that of state-of-the-art catalysts. Recyclability and stability studies confirmed that the catalyst was not only easily recoverable from the reaction environment but also possessed high stability and good reusability after a long period of time. The results of this study showed that the family of Au/NH_2-SiO_2-shell/Fe_3O_4-core catalysts is promising toward the heterogenization of Au, easily recoverability of catalysts, and conversion of nitro aromatic compounds in aqueous phase either from an environmental or industrial point of view.

4. EXPERIMENTAL DETAILS

4.1. Materials. Iron(III) chloride anhydrous (98%), toluene (99.5%), and ethanol (99.9%) were purchased from Merck (India). Chloroauric acid (99%) was obtained from Loba Chemie (India). Ammonia solution (30% NH_3 in water) was purchased from Qualigen Fine Chemicals (India). 3-Aminopropyltriethoxysilane (APTES, 99%) was obtained from Sigma-Aldrich (Germany). Tetraethyl orthosilicate (TEOS) was procured (98%) from Acros. All chemicals were used as received without any further purification.

4.2. Catalyst Synthesis. *4.2.1. Synthesis of Fe_3O_4 Nanoparticles.* $FeCl_3$ (3.25 g), 1.3 g of trisodium citrate, and 6 g of sodium acetate were added to 50 cm^3 of ethylene glycol solution, which results in the formation of a yellow solution, followed by stirring for 1 h. Then, the whole solution was subjected to hydrothermal treatment at 473 K for 10 h in a Teflon-lined autoclave. After that, the resultant solids were separated and washed three times with an ethanol−water mixture. Then, the solids were dried under vacuum at 333 K for 12 h.[64]

4.2.2. Preparation of Fe_3O_4@SiO_2 Microspheres. Synthesized Fe_3O_4 (20 mg) was added to a sealed round-bottom flask containing 120 cm^3 of ethanol and 18 cm^3 of deionized water and sonicated for 15 min in an Ar atmosphere. Then, 7.5 cm^3 of 28% aqueous solution of NH_3 was added to it, followed by the slow addition of 3.8 cm^3 of TEOS for 10 min. This mixture was subjected to mechanical stirring for 10 h, after which the resultant precipitate was separated and washed three times with an ethanol and water mixture. Finally, the resulting solids were dried under vacuum at 333 K for 12 h.[65]

4.2.3. Amine Modification. The dry support material (0.5 g) was added to a sealed round-bottom flask containing 50 cm^3 of toluene and sonicated (ultrasonic bath, Fischer Scientific) under an Ar atmosphere. Then, 0.7 cm^3 of APTES was added under a slow stirring condition and refluxed at 393 K for 12 h. After this step, the resultant solids were separated and washed three times with an ethanol−water mixture. Finally, the solid was dried in a vacuum oven (LabTech) at 318 K for 12 h.[66]

4.2.4. Gold Deposition. The support material (0.5 g) was added to a solution containing 150 cm^3 of H_2O and 0.035 g of chloroauric acid under stirring. Then, 5 cm^3 of a freshly prepared 0.1 M $NaBH_4$ solution was added to the previous solution, which resulted in a rapid color change from buff to wine red. After this step, the resultant solid was separated and washed three times with an ethanol−water mixture. The resulting solid was then dried under vacuum at 323 K for 12 h.[67] The comprehensive synthesis process of the as-prepared Au/NH_2-SiO_2-shell/Fe_3O_4-core is depicted in Figure S1.

4.3. Characterization. Nitrogen adsorption−desorption isotherms were measured at liquid nitrogen temperature (∼77 K) with a Quantachrome Nova-3200e instrument. Samples were pretreated at 573 K for 6 h under high vacuum. The surface area was determined by the Brunauer−Emmett−Teller (BET) method. The pore size distributions were calculated from the isotherm desorption branch using the Barrett−Joyner−Halenda model. XRD patterns and catalyst crystalline phases were recorded and identified at ambient temperature on an X-ray diffractometer (Bruker AXS D-8, Advanced SWAX) using Cu Kα radiation (0.15406 nm) as the X-ray source. Peaks were identified by a search-match technique using X'Pert HighScore Plus software with reference to the JCPDS database. The HR-TEM investigation was done by a JEOL JEM 2100 microscope operated at 200 kV acceleration voltage using a lacey carbon-coated Cu grid of 300 mesh size. UV−vis spectroscopic measurements were carried out with a UV-2450 spectrometer (Shimadzu). The FTIR spectra were recorded with a PerkinElmer GX spectrometer. The spectra were recorded in the range of 400−4000 cm^{-1} using the KBr pellet technique.

■ ASSOCIATED CONTENT

Supporting Information

The Supporting Information is available free of charge on the ACS Publications website at DOI: 10.1021/acsomega.8b03655.

Formation of a magnetically recyclable Fe_3O_4@SiO_2-NH_2−Au microsphere (PDF)

■ AUTHOR INFORMATION

Corresponding Authors

*E-mail: jjbravo@ku.edu (J.J.B.-S.).
*E-mail: biswajit72@iitism.ac.in. Phone +91-326-223-5663, (+91)-326-2296563 (B.C.).

ORCID

Juan J. Bravo-Suárez: 0000-0002-6484-374X
Biswajit Chowdhury: 0000-0003-3257-2065

Author Contributions

⊥K.B. and B.D.D. have equal contribution in the work.

DOI: 10.1021/acsomega.8b03655
ACS Omega 2019, 4, 4071−4081

Notes

The authors declare no competing financial interest.
[#]Formerly at NIT Jamshedpur, Jharkhand (R.K.).

■ ACKNOWLEDGMENTS

K.B. and B.D.D. would like to acknowledge IIT (ISM) for providing research fellowship. S.C. would like to acknowledge DST for funding under Inspire Scheme. B.C. would like to acknowledge SERB, DST, Govt of India, for funding under the Scheme No. SB/S1/PC-10/2012. J.J.B.-S. acknowledges financial support by the National Science Foundation, grant no. OIA-1539105.

■ REFERENCES

(1) Chang, Y.-C.; Chen, D.-H. Catalytic reduction of 4-nitrophenol by magnetically recoverable Au nanocatalyst. *J. Hazard. Mater.* **2009**, *165*, 664−669.
(2) Chiou, J.-R.; Lai, B.-H.; Hsu, K.-C.; Chen, D.-H. One-pot green synthesis of silver/iron oxide composite nanoparticles for 4-nitrophenol reduction. *J. Hazard. Mater.* **2013**, *248*−*249*, 394−400.
(3) Pachfule, P.; Kandambeth, S.; Díaz Díaz, D.; Banerjee, R. Highly stable covalent organic framework−Au nanoparticles hybrids for enhanced activity for nitrophenol reduction. *Chem. Commun.* **2014**, *50*, 3169−3172.
(4) Wu, W.; Liang, S.; Chen, Y.; Shen, L.; Zheng, H.; Wu, L. High efficient photocatalytic reduction of 4-nitroaniline to p-phenylenediamine over microcrystalline $SrBi_2Nb_2O_9$. *Catal. Commun.* **2012**, *17*, 39−42.
(5) Smiley, R. A. Phenylene-and Toluenediamines. In *Ullmann's Encyclopedia of Industrial Chemistry*; Wiley, 2002; Vol. *26*.
(6) Sharma, R. K.; Monga, Y.; Puri, A. Magnetically separable silica@Fe_3O_4 core−shell supported nano-structured copper(II) composites as a versatile catalyst for the reduction of nitroarenes in aqueous medium at room temperature. *J. Mol. Catal. A: Chem.* **2014**, *393*, 84−95.
(7) Apolinário, Â. C.; Silva, A. M. T.; Machado, B. F.; Gomes, H. T.; Araújo, P. P.; Figueiredo, J. L.; Faria, J. L. Wet air oxidation of nitroaromatic compounds: Reactivity on single- and multi-component systems and surface chemistry studies with a carbon xerogel. *Appl. Catal., B* **2008**, *84*, 75−86.
(8) Polat, K.; Aksu, M. L.; Pekel, A. T. Electroreduction of nitrobenzene to p-aminophenol using voltammetric and semipilot scale preparative electrolysis techniques. *J. Appl. Electrochem.* **2002**, *32*, 217−223.
(9) Chu, Y. Y.; Qian, Y.; Wang, W. J.; Deng, X. L. A dual-cathode electro-Fenton oxidation coupled with anodic oxidation system used for 4-nitrophenol degradation. *J. Hazard. Mater.* **2012**, *199*−*200*, 179−185.
(10) Dai, R.; Chen, J.; Lin, J.; Xiao, S.; Chen, S.; Deng, Y. Reduction of nitro phenols using nitroreductase from *E. coli* in the presence of NADH. *J. Hazard. Mater.* **2009**, *170*, 141−143.
(11) She, Z.; Gao, M.; Jin, C.; Chen, Y.; Yu, J. Toxicity and biodegradation of 2,4-dinitrophenol and 3-nitrophenol in anaerobic systems. *Process Biochem.* **2005**, *40*, 3017−3024.
(12) Deraedt, C.; Salmon, L.; Gatard, S.; Ciganda, R.; Hernandez, R.; Ruiz, J.; Astruc, D. Sodium borohydride stabilizes very active gold nanoparticle catalysts. *Chem. Commun.* **2014**, *50*, 14194−14196.
(13) Shin, K. S.; Cho, Y. K.; Choi, J.-Y.; Kim, K. Facile synthesis of silver-deposited silanized magnetite nanoparticles and their application for catalytic reduction of nitrophenols. *Appl. Catal., A* **2012**, *413*−*414*, 170−175.
(14) Goyal, A.; Bansal, S.; Singhal, S. Facile reduction of nitrophenols: Comparative catalytic efficiency of MFe_2O_4 (M = Ni, Cu, Zn) nano ferrites. *Int. J. Hydrogen Energy* **2014**, *39*, 4895−4908.
(15) Feng, J.; Su, L.; Ma, Y.; Ren, C.; Guo, Q.; Chen, X. $CuFe_2O_4$ magnetic nanoparticles: A simple and efficient catalyst for the reduction of nitrophenol. *Chem. Eng. J.* **2013**, *221*, 16−24.
(16) Chen, Y.; Zhang, Y.; Kou, Q.; Liu, Y.; Han, D.; Wang, D.; Sun, Y.; Zhang, Y.; Wang, Y.; Lu, Z.; Chen, L.; Yang, J.; Xing, S. Enhanced Catalytic Reduction of 4-Nitrophenol Driven by Fe_3O_4-Au Magnetic Nanocomposite Interface Engineering: From Facile Preparation to Recyclable Application. *Nanomaterials* **2018**, *8*, 353.
(17) Kureha, T.; Nagase, Y.; Suzuki, D. High Reusability of Catalytically Active Gold Nanoparticles Immobilized in Core−Shell Hydrogel Microspheres. *ACS Omega* **2018**, *3*, 6158−6165.
(18) Nasrollahzadeh, M.; Sajadi, S. M.; Rostami-Vartooni, A.; Bagherzadeh, M.; Safari, R. Immobilization of copper nanoparticles on perlite: Green synthesis, characterization and catalytic activity on aqueous reduction of 4-nitrophenol. *J. Mol. Catal. A: Chem.* **2015**, *400*, 22−30.
(19) Veisi, H.; Ghorbani-Vaghei, R.; Hemmati, S.; Aliani, M. H.; Ozturk, T. Green and effective route for the synthesis of monodispersed palladium nanoparticles using herbal tea extract (*Stachys lavandulifolia*) as reductant, stabilizer and capping agent, and their application as homogeneous and reusable catalyst in Suzuki coupling reactions in water. *Appl. Organomet. Chem.* **2015**, *29*, 26−32.
(20) Astruc, D.; Lu, F.; Aranzaes, J. R. Nanoparticles as Recyclable Catalysts: The Frontier between Homogeneous and Heterogeneous Catalysis. *Angew. Chem., Int. Ed.* **2005**, *44*, 7852−7872.
(21) Masatake, H.; Tetsuhiko, K.; Hiroshi, S.; Nobumasa, Y. Novel Gold Catalysts for the Oxidation of Carbon Monoxide at a Temperature far Below 0 °C. *Chem. Lett.* **1987**, *16*, 405−408.
(22) Kanungo, S.; Keshri, K. S.; van Hoof, A. J. F.; d'Angelo, M. F. N.; Schouten, J. C.; Nijhuis, T. A.; Hensen, E. J. M.; Chowdhury, B. Silylation enhances the performance of Au/Ti−SiO_2 catalysts in direct epoxidation of propene using H_2 and O_2. *J. Catal.* **2016**, *344*, 434−444.
(23) Chowdhury, B.; Bravo-Suárez, J. J.; Daté, M.; Tsubota, S.; Haruta, M. Trimethylamine as a Gas-Phase Promoter: Highly Efficient Epoxidation of Propylene over Supported Gold Catalysts. *Angew. Chem., Int. Ed.* **2006**, *45*, 412−415.
(24) Hutchings, G. J. Vapor phase hydrochlorination of acetylene: Correlation of catalytic activity of supported metal chloride catalysts. *J. Catal.* **1985**, *96*, 292−295.
(25) Sobczak, I.; Jagodzinska, K.; Ziolek, M. Glycerol oxidation on gold catalysts supported on group five metal oxides—A comparative study with other metal oxides and carbon based catalysts. *Catal. Today* **2010**, *158*, 121−129.
(26) Santra, C.; Rahman, S.; Bojja, S.; James, O. O.; Sen, D.; Maity, S.; Mohanty, A. K.; Mazumder, S.; Chowdhury, B. Barium, calcium and magnesium doped mesoporous ceria supported gold nanoparticle for benzyl alcohol oxidation using molecular O_2. *Catal. Sci. Technol.* **2013**, *3*, 360−370.
(27) Esmaeilpour, M.; Sardarian, A. R.; Javidi, J. Schiff base complex of metal ions supported on superparamagnetic Fe_3O_4@SiO_2 nanoparticles: An efficient, selective and recyclable catalyst for synthesis of 1,1-diacetates from aldehydes under solvent-free conditions. *Appl. Catal., A* **2012**, *445*−*446*, 359−367.
(28) Zhang, M.; Zhu, X.; Liang, X.; Wang, Z. Preparation of highly efficient Au/C catalysts for glucose oxidation via novel plasma reduction. *Catal. Commun.* **2012**, *25*, 92−95.
(29) Purushothaman, R. K. P.; van Haveren, J.; van Es, D. S.; Melián-Cabrera, I.; Meeldijk, J. D.; Heeres, H. J. An efficient one pot conversion of glycerol to lactic acid using bimetallic gold-platinum catalysts on a nanocrystalline CeO_2 support. *Appl. Catal., B* **2014**, *147*, 92−100.
(30) Esken, D.; Turner, S.; Lebedev, O. I.; Van Tendeloo, G.; Fischer, R. A. Au@ZIFs: Stabilization and Encapsulation of Cavity-Size Matching Gold Clusters inside Functionalized Zeolite Imidazolate Frameworks, ZIFs. *Chem. Mater.* **2010**, *22*, 6393−6401.
(31) Le, X.; Dong, Z.; Zhang, W.; Li, X.; Ma, J. Fibrous nano-silica containing immobilized Ni@Au core−shell nanoparticles: A highly active and reusable catalyst for the reduction of 4-nitrophenol and 2-nitroaniline. *J. Mol. Catal. A: Chem.* **2014**, *395*, 58−65.
(32) Banazadeh, A.; Pirisedigh, A.; Aryanasab, F.; Salimi, H.; Shafiei-Haghighi, S. Novel synthesis and characterization of Fe_3O_4@silica−

DOI: 10.1021/acsomega.8b03655
ACS Omega 2019, 4, 4071−4081

palladium nanocatalyst: A highly active and reusable heterogeneous catalyst for Heck cross-coupling reactions. *Inorg. Chim. Acta* **2015**, *429*, 132−137.
(33) Patra, A. K.; Dutta, A.; Bhaumik, A. Mesoporous Core−Shell Fenton Nanocatalyst: A Mild, Operationally Simple Approach to the Synthesis of Adipic Acid. *Chem. - Eur. J.* **2013**, *19*, 12388−12395.
(34) Duan, X.; Liu, J.; Hao, J.; Wu, L.; He, B.; Qiu, Y.; Zhang, J.; He, Z.; Xi, J.; Wang, S. Magnetically recyclable nanocatalyst with synergetic catalytic effect and its application for 4-nitrophenol reduction and Suzuki coupling reactions. *Carbon* **2018**, *130*, 806−813.
(35) Mohammadi, P.; Sheibani, H. Green synthesis of Fe_3O_4@SiO_2-Ag magnetic nanocatalyst using safflower extract and its application as recoverable catalyst for reduction of dye pollutants in water. *Appl. Organomet. Chem.* **2018**, *32*, No. e4249.
(36) Zheng, J.; Dong, Y.; Wang, W.; Ma, Y.; Hu, J.; Chen, X.; Chen, X. In situ loading of gold nanoparticles on Fe_3O_4@SiO_2 magnetic nanocomposites and their high catalytic activity. *Nanoscale* **2013**, *5*, 4894−4901.
(37) Rahman, Z. U.; Zhang, T.; Cui, S.; Wang, D. Preparation and characterization of magnetic nanocomposite catalysts with double Au nanoparticle layers. *RSC Adv.* **2015**, *5*, 99697−99705.
(38) Walker, J. M.; Zaleski, J. M. A simple route to diverse noble metal-decorated iron oxide nanoparticles for catalysis. *Nanoscale* **2016**, *8*, 1535−1544.
(39) Lin, F.-h.; Doong, R.-a. Highly efficient reduction of 4-nitrophenol by heterostructured gold-magnetite nanocatalysts. *Appl. Catal., A* **2014**, *486*, 32−41.
(40) Du, X.; He, J. Amino-functionalized silica nanoparticles with center-radially hierarchical mesopores as ideal catalyst carriers. *Nanoscale* **2012**, *4*, 852−859.
(41) Dong, Z.; Le, X.; Li, X.; Zhang, W.; Dong, C.; Ma, J. Silver nanoparticles immobilized on fibrous nano-silica as highly efficient and recyclable heterogeneous catalyst for reduction of 4-nitrophenol and 2-nitroaniline. *Appl. Catal., B* **2014**, *158−159*, 129−135.
(42) Fang, J.; Zhang, Y.; Zhou, Y.; Zhao, S.; Zhang, C.; Huang, M.; Gao, Y.; Yang, C. Synthesis of double-shell hollow magnetic Au-loaded ellipsoids as highly active and recoverable nanoreactors. *New J. Chem.* **2017**, *41*, 4448−4457.
(43) Sun, Z.; Li, H.; Cui, G.; Tian, Y.; Yan, S. Multifunctional magnetic core−shell dendritic mesoporous silica nanospheres decorated with tiny Ag nanoparticles as a highly active heterogeneous catalyst. *Appl. Surf. Sci.* **2016**, *360*, 252−262.
(44) Ucoski, G. M.; Nunes, F. S.; DeFreitas-Silva, G.; Idemori, Y. M.; Nakagaki, S. Metalloporphyrins immobilized on silica-coated Fe_3O_4 nanoparticles: Magnetically recoverable catalysts for the oxidation of organic substrates. *Appl. Catal., A* **2013**, *459*, 121−130.
(45) Thommes, M.; Kaneko, K.; Neimark Alexander, V.; Olivier James, P.; Rodriguez-Reinoso, F.; Rouquerol, J.; Sing Kenneth, S. W. Physisorption of gases, with special reference to the evaluation of surface area and pore size distribution (IUPAC Technical Report). *Pure Appl. Chem.* **2015**, *87*, 9−10.
(46) Zhao, W.; Gu, J.; Zhang, L.; Chen, H.; Shi, J. Fabrication of Uniform Magnetic Nanocomposite Spheres with a Magnetic Core/Mesoporous Silica Shell Structure. *J. Am. Chem. Soc.* **2005**, *127*, 8916−8917.
(47) Mahto, T. K.; Chandra, S.; Haldar, C.; Sahu, S. K. Kinetic and thermodynamic study of polyaniline functionalized magnetic mesoporous silica for magnetic field guided dye adsorption. *RSC Adv.* **2015**, *5*, 47909−47919.
(48) Mandal, S.; Santra, C.; Kumar, R.; Pramanik, M.; Rahman, S.; Bhaumik, A.; Maity, S.; Sen, D.; Chowdhury, B. Niobium doped hexagonal mesoporous silica (HMS-X) catalyst for vapor phase Beckmann rearrangement reaction. *RSC Adv.* **2014**, *4*, 845−854.
(49) Manakhov, A.; Čechal, J.; Michlíček, M.; Shtansky, D. V. Determination of NH_2 concentration on 3-aminopropyl tri-ethoxy silane layers and cyclopropylamine plasma polymers by liquid-phase derivatization with 5-iodo 2-furaldehyde. *Appl. Surf. Sci.* **2017**, *414*, 390−397.
(50) Evangelista, V.; Acosta, B.; Miridonov, S.; Smolentseva, E.; Fuentes, S.; Simakov, A. Highly active Au-CeO_2@ZrO_2 yolk−shell nanoreactors for the reduction of 4-nitrophenol to 4-aminophenol. *Appl. Catal., B* **2015**, *166−167*, 518−528.
(51) Gupta, V. K.; Atar, N.; Yola, M. L.; Üstündağ, Z.; Uzun, L. A novel magnetic Fe@Au core−shell nanoparticles anchored graphene oxide recyclable nanocatalyst for the reduction of nitrophenol compounds. *Water Res.* **2014**, *48*, 210−217.
(52) Li, N.; Echeverría, M.; Moya, S.; Ruiz, J.; Astruc, D. "Click" Synthesis of Nona-PEG-branched Triazole Dendrimers and Stabilization of Gold Nanoparticles That Efficiently Catalyze p-Nitrophenol Reduction. *Inorg. Chem.* **2014**, *53*, 6954−6961.
(53) Rocha, M.; Fernandes, C.; Pereira, C.; Rebelo, S. L. H.; Pereira, M. F. R.; Freire, C. Gold-supported magnetically recyclable nanocatalysts: a sustainable solution for the reduction of 4-nitrophenol in water. *RSC Adv.* **2015**, *5*, 5131−5141.
(54) Gatard, S.; Salmon, L.; Deraedt, C.; Ruiz, J.; Astruc, D.; Bouquillon, S. Gold Nanoparticles Stabilized by Glycodendrimers: Synthesis and Application to the Catalytic Reduction of 4-Nitrophenol. *Eur. J. Inorg. Chem.* **2014**, *2014*, 2671−2677.
(55) Gupta, S. S. R.; Kantam, M. L.; Bhanage, B. M. Shape-selective synthesis of gold nanoparticles and their catalytic activity towards reduction of p-nitroaniline. *Nano-Struct. Nano-Objects* **2018**, *14*, 125−130.
(56) Takei, T.; Akita, T.; Nakamura, I.; Fujitani, T.; Okumura, M.; Okazaki, K.; Huang, J.; Ishida, T.; Haruta, M. Heterogeneous Catalysis by Gold. In *Adv. Catal.*; Gates, B. C.; Jentoft, F. C., Eds.; Academic Press, 2012; Chapter 1, Vol. *55*; pp 1−126.
(57) Shekhar, M.; Wang, J.; Lee, W.-S.; Williams, W. D.; Kim, S. M.; Stach, E. A.; Miller, J. T.; Delgass, W. N.; Ribeiro, F. H. Size and Support Effects for the Water−Gas Shift Catalysis over Gold Nanoparticles Supported on Model Al_2O_3 and TiO_2. *J. Am. Chem. Soc.* **2012**, *134*, 4700−4708.
(58) Wu, H.; Huang, X.; Gao, M.; Liao, X.; Shi, B. Polyphenol-grafted collagen fiber as reductant and stabilizer for one-step synthesis of size-controlled gold nanoparticles and their catalytic application to 4-nitrophenol reduction. *Green Chem.* **2011**, *13*, 651−658.
(59) Lin, C.; Tao, K.; Hua, D.; Ma, Z.; Zhou, S. Size Effect of Gold Nanoparticles in Catalytic Reduction of p-Nitrophenol with $NaBH_4$. *Molecules* **2013**, *18*, 12609.
(60) Yang, H.; Li, S.; Zhang, X.; Wang, X.; Ma, J. Imidazolium ionic liquid-modified fibrous silica microspheres loaded with gold nanoparticles and their enhanced catalytic activity and reusability for the reduction of 4-nitrophenol. *J. Mater. Chem. A* **2014**, *2*, 12060−12067.
(61) Chiu, C.-Y.; Chung, P.-J.; Lao, K.-U.; Liao, C.-W.; Huang, M. H. Facet-Dependent Catalytic Activity of Gold Nanocubes, Octahedra, and Rhombic Dodecahedra toward 4-Nitroaniline Reduction. *J. Phys. Chem. C* **2012**, *116*, 23757−23763.
(62) Thomas, M.; Sheikh, M. U. D.; Ahirwar, D.; Bano, M.; Khan, F. Gold nanoparticle and graphene oxide incorporated strontium crosslinked alginate/carboxymethyl cellulose composites for o-nitroaniline reduction and Suzuki-Miyaura cross-coupling reactions. *J. Colloid Interface Sci.* **2017**, *505*, 115−129.
(63) Liu, B.; Yang, M.; Li, H. Synthesis of gold nanoflowers assisted by a CH-CF hybrid surfactant and their applications in SERS and catalytic reduction of 4-nitroaniline. *Colloids Surf., A* **2017**, *520*, 213−221.
(64) Xuan, S.; Wang, Y.-X. J.; Leung, K. C.-F.; Shu, K. Synthesis of Fe_3O_4@Polyaniline Core/Shell Microspheres with Well-Defined Blackberry-Like Morphology. *J. Phys. Chem. C* **2008**, *112*, 18804−18809.
(65) Li, W.; Yang, J.; Wu, Z.; Wang, J.; Li, B.; Feng, S.; Deng, Y.; Zhang, F.; Zhao, D. A Versatile Kinetics-Controlled Coating Method To Construct Uniform Porous TiO_2 Shells for Multifunctional Core−Shell Structures. *J. Am. Chem. Soc.* **2012**, *134*, 11864−11867.
(66) Srivastava, R.; Srinivas, D.; Ratnasamy, P. CO_2 activation and synthesis of cyclic carbonates and alkyl/aryl carbamates over adenine-modified Ti-SBA-15 solid catalysts. *J. Catal.* **2005**, *233*, 1−15.

DOI: 10.1021/acsomega.8b03655
ACS Omega 2019, 4, 4071−4081

(67) Zhu, Y.; Shen, J.; Zhou, K.; Chen, C.; Yang, X.; Li, C. Multifunctional Magnetic Composite Microspheres with in Situ Growth Au Nanoparticles: A Highly Efficient Catalyst System. *J. Phys. Chem. C* **2011**, *115*, 1614−1619.

DOI: 10.1021/acsomega.8b03655
ACS Omega 2019, 4, 4071−4081